A Supramolecular Approach to Develop New Soybean and Lupin Peptide Nanogels with Enhanced Dipeptidyl Peptidase IV (DPP-IV) Inhibitory Activity

Raffaele Pugliese[1,2], Carlotta Bollati[3], Fabrizio Gelain[1,2], Anna Arnoldi[3], Carmen Lammi[3*]

[1]Tissue Engineering Unit, Institute for Stem Cell Biology, Regenerative Medicine and Innovative Therapies-ISBReMIT, Fondazione IRCSS Casa Sollievo della Sofferenza, San Giovanni Rotondo (FG), Italy

[2]Center for Nanomedicine and Tissue Engineering (CNTE), ASST Grande Ospedale Metropolitano Niguarda, Milan, Italy

[3]Department of Pharmaceutical Sciences, University of Milan, Milan, Italy

* Correspondence: Phone: +39-0250319372; FAX: +39-0250319359; Email: carmen.lammi@unimi.it.

Abstract

Soy1 (IAVPTGVA) and Lup1 (LTFPGSAED), two peptides from soybean and lupin protein hydrolysis, have been singled out as dipeptidyl peptidase IV (DPP-IV) activity inhibitors in different model systems. However, their activity is affected by their instability toward intestinal proteases. Here, an innovative strategy based on nanogels was developed in order to increase both their stability and anti-diabetic properties, through encapsulation into the RADA16 peptide. The nanogel formation was stimulated by a solvent-triggered approach, allowing us to produce stable nanogels (G'=1826 Pa, stress-failure $\geq$ 50 Pa) with shear-thinning propensity. ThT binding assay, and ATR-FTIR spectroscopy experiments showed that nanogels self-aggregated into stable cross-β structures providing higher resistance against proteases (*ex vivo* experiments) and increased bioavailability of Soy1 and Lup1 peptides (*in situ* experiments on Caco-2 cells). Hence, this simple and harmless nanotechnological approach could be a key-step in making innovative nanomaterials for nutraceuticals delivering.

Keywords: bioactive peptides, dipeptidyl peptidase IV inhibitor, nano-nutraceutical, nanogel, rheology, self-assembling peptide, supramolecular chemistry

INTRODUCTION

Dipeptidyl peptidase IV (DPP-IV)/CD26 is a serine exopeptidase (EC 3.4.14.5) expressed on the surface of most cells (renal proximal tubules, intestinal epithelial cells, and vascular endothelium).[1] Moreover, a soluble form of this enzyme is also known as a product of the proteolytic cleavage of the membrane enzyme and its levels and/or activity have been correlated with many diseases, such as type 2 diabetes (T2DM) and cardiovascular disease.[2, 3]

DPP-IV plays an important role in glucose metabolism regulation, and for this reason it is now considered a novel anti-diabetic target.[4] Among its substrates, DPP-IV is responsible for the degradation of glucagon-like peptide (GLP-1) and gastrointestinal insulinotropic peptide (GIP), which are also known as incretins.[5] After meal ingestion, GLP-1 and GIP are released by the gut and they promote the insulin biosynthesis and secretion at pancreatic levels;[5] however, they show a very low half-life at plasmatic level, since they are rapidly metabolized by DPP-IV activity.[6] Therefore, DPP-IV inhibitors have emerged as a new class of oral antidiabetic agents,[6, 7] and numerous researches are looking for novel food-derived peptides as natural DPP-IV inhibitors.[4, 8-10]

In this context, we have identified two peptides deriving from the cleavage of plant proteins endowed by a DPP-IV inhibitory activity.[11] The former named Lup1 or P7[12] (LTFPGSAED) derives from beta-conglutin, a lupin 7S globulin, whereas the latter named Soy1 (IAVPTGVA). derives from glycinin, a soybean 11S globulin.

We have demonstrated that both peptides inhibit *in vitro* the activity of human DPP-IV with regular dose-response relationships and IC_{50} values equal to 228 and 106 μM.[11] Moreover, a molecular docking analysis has permitted to predict the key molecular interactions that stabilize the active conformations of Lup1 and Soy1 within the DPP-IV enzyme site.[11]

These preliminary results have prompted us to extend the investigation to other model systems of the inhibition of the DPP-IV activity. In fact, we have specifically developed and optimized either a

cellular assay using undifferentiated Caco-2 cells or an *ex vivo* one based on human serum samples.[13] Our findings have clearly indicated that both peptides inhibit the DPP-IV activity in Caco-2 cell in a dose-dependent manner, displaying IC_{50} values of 208 µM in case of Lup1 and 223 µM in case of Soy1, respectively. In addition, tested at a 100 µM concentration, these peptides inhibit the circulating form of DPP-IV by 18.1% and 27.7%, respectively.[13]

However, other investigations have shown that, even if intestinal cells[14, 15] absorb both peptides, after 2 h of incubation Soy1 is partially degraded by the active protease expressed on the apical surface of differentiated Caco-2 cells.[15] Since the low stability and bioavailability impair the development of any practical applications of these peptides, the use of well-designed and controlled delivery systems based on supramolecular chemistry might represent a useful approach to overcome this critical issue.[16, 17]

In this context, self-assembling peptide-based hydrogels (SAPs) are able to deliver bioactive compounds in a controlled manner.[18-22] In general, SAPs are short peptides (8-16 residues) containing alternate charged hydrophilic and hydrophobic amino acids that spontaneously self-organize into interwoven nanofibers with diameters of 10-20 nm.[21] This free energy driven process can be readily and finely tuned by molecular chemistry (i.e. co-assembling molecules), assembling conditions (pH, temperature, solvents, or electrolytes), and assembly kinetics.[21] The design versatility of peptide building blocks, in combination with their ability to adopt specific secondary structures, provides a suitable platform for the design of nanomaterials with controlled structural features at the nanoscale level. Additionally, peptide hydrogels are easy to use, biodegradable, non-toxic, non-immunogenic, and non-thrombogenic.

In light of these observations, it was decided to enhance the stability of peptides Lup1 and Soy1 by combining them with the ionic self-complementary RADA16 peptide (i.e. Ac-RADARADARADARADA-$CONH_2$), a well know and characterized SAP based-hydrogel[23] as a strategy to develop new nanogel formulations, having already applied successfully the same kind of approach for enhancing the activity of hempseed protein hydrolysates.[24] This approach allowed us to

produce nanofibrous tryptic and peptic hempseed hydrolysate-RADA16 based hydrogels with an increase of 2.0 folds of the DPP-IV inhibitory activities in respect to the plain solutions. In particular, trapped inside the entangled nanofibrous domains of the hydrogels, hempseed peptides are slowly released allowing the interaction with the DPP-IV enzyme, expressed on the surface of human intestinal Caco-2 cells. Further, this nano-formulation was used as a delivery system of the antidiabetic drug sitagliptin, helping to reduce its dosage and eventually associated side effects.

Here, new RADA16-based nanogels were developed as smart delivery systems of both Lup1 and Soy1 peptides with the objective of reducing the concentrations needed for the DPP-IV inhibition. Rheological, ThT binding assay, and ATR-FTIR experiments showed the feasibility of this encapsulation procedure. Then, the kinetic of the peptide release from the nanogels was evaluated as a function of time, and their enhanced bioactivity as DPP-IV inhibitors was pursued by performing *in situ* and *ex vivo* experiments.

MATERIALS AND METHODS

All reagents and solvents used for the peptide synthesis were purchased from commercial sources and used without any further purification. See "Supplementary Materials" for further details on materials and methods.

Peptide Synthesis. RADA16 peptides were synthesized on solid support using a Rink amide 4-methyl-benzhydrylamine resin (0.5 mmol g^{-1} substitution). Following synthesis, the peptides were cleaved from the resin using a 95:2.5:2.5 mixture of TFA:TIS:H_2O, and precipitated using cold diethyl ether. The resulting raw peptides were purified using a Waters binary high-performance liquid chromatography (HPLC) apparatus (>95%). The purity and the molecular weight of the peptides were confirmed via single quadrupole mass detection (LC-MS Alliance-3100, Waters, Sesto San Giovanni, Italy). Purified peptides were lyophilized and stored at -20°C. The peptides Soy1 and Lup1 were synthesized by the company PRIMM (Milan, Italy) with >95% purity assessed by HPLC.

Preparation of Soy1 and Lupin1 Nanogels. The purified RADA16 was dissolved at 10 mg mL^{-1} in distilled water (Gibco®, Thermo Fisher Scientific,Waltham, MA USA), sonicated for 30 min, and incubated at 4 °C for 24 h. Subsequently, the encapsulation of Lup1 and Soy1 (0.1-1000.0 μM concentration range) was performed. Then, the mixed solutions were stirred for 2 min at room temperature (RT) in order to obtain homogeneous transparent solutions. During this process no precipitation of the RADA16 or Lup1 and Soy1 peptides was observed. In order to prepare the gel samples a solvent-triggered approach was used: PBS 1X (Ca^{2+}/Mg^{2+} free) or DMEM (typically ~20 μL) were added in the mixed solutions in order to obtain a nanogel state.

Spectroscopic Analysis. FT-IR analysis of assembled nanostructures was performed on peptides dissolved at a concentration of 1% (w/v) in distilled water (Gibco®), after 24 h incubation at 4 °C, as previously described.[25] All the collected spectra were reported after ATR correction, smoothing and automatic baseline correction using Origin™8 software. Each sample preparation was repeated three times.

Thioflavin T (ThT) Spectroscopy Assay. In order to assess the presence of cross-β fibril structures, ThT analysis of assembled peptides was performed. Peptides at 1% (w/v) were mixed with ThT working solution (1:0.5v/v) and stirred for 2 min. ThT binding was recorded using an Infinite M200 PRO plate reader (Tecan, Männedorf, Switzerland) with λ_{ex} = 440 nm (5 nm bandpass) and λ_{em} = 482 nm (10 nm bandpass), over 60 s at 25 °C. Each sample was analyzed in triplicate, normalized by ThT fluorescence alone, and processed with Origin™8 software.

Rheological Tests. Rheological properties of assembled nanostructures were assessed using a controlled stress AR-2000ex Rheometer (TA instruments, New Castle, DE, USA) with a truncated

cone-plate geometry (acrylic truncated diameter, 20 mm; angle, 1°; truncation gap, 34 μm). All measurements were obtained at 25 °C. All samples were tested 24 h after dissolution at the concentration of 1% (w/v). To monitor the sol-gel transition and to evaluate the storage (*G'*) and loss (*G"*) moduli increase as a function of time, a time-sweep test at constant angular frequency (ω= 1 Hz) was carried out for 10 h. The assembly of all samples was triggered by adding PBS (Ca^{2+}/Mg^{2+} free) laterally to the peptide solution positioned in the 34 μm cone-plate truncation gap. Afterwards, Frequency sweep experiments were recorded as a function angular frequency (0.1-100 Hz) at a fixed strain of 1%. Stress/strain sweeps were performed on samples from 0.01% to a maximum strain of 1000% for determining the limit of the linear viscoelastic region and the maximum stress/strain to which the sample can be subjected. Lastly, to test the injectability of peptide solutions, shear-thinning tests were performed by a series of peak hold tests in which shear rates were kept constant, as previously reported. Briefly, firstly a shear rate of 0.01 s^{-1} was applied for 60 s, and then a shear rate of 5.3 s^{-1} was applied for 20 s, for simulating the shear rate inside the syringe barrel. Subsequently, a high shear rate of 1000 s^{-1} was applied for 20 s to simulate the purge injection of the solution. Afterwards a shear rate of 5.3 s^{-1} (20 s) was applied again, thus mimicking the flow of peptide solution out of the needle. Lastly, a shear rate of 0.01 s^{-1} was performed in order to simulate the low shear condition of the solution during injection. Each experiment was performed in triplicate.

Cell Culture. Caco-2 cells, obtained from Institut National de la Santé et de la Recherche Médicale (INSERM, Paris), were routinely sub-cultured at 50% density and were maintained at 37 °C in a 90% air–10% CO_2 atmosphere in Dulbecco Minimum Essential Medium (DMEM) containing 25 mM glucose, 3.7 g L^{-1} $NaHCO_3$, 4 mM stable L-glutamine, 1% nonessential amino acids, 100 U L^{-1} penicillin, 100 μg L^{-1} streptomycin (complete medium), supplemented with 10% heat-inactivated fetal bovine serum (FBS Hyclone Laboratories, Logan, UT, USA).

***In situ* DPPIV Activity Assay.** A total of 5×10^4/well Caco-2 cells were seeded on the surface of the

RADA16-Lup1 and RADA16-Soy1 (0.1-1000.0 μM) nanogels in black 96-well plates with clear bottom. The following day, the spent media were removed and cells were washed with 100.0 μL of PBS (Ca^{2+}/Mg^{2+} free), and 100.0 μL of Gly-Pro-AMC substrate at the concentration of 50.0 μM in PBS (Ca^{2+}/Mg^{2+} free) were added in each well. Fluorescence signals (ex./em. 350/450 nm) were measured using a Synergy H1 instrument (Biotek, Bad Friedrichshall, Germany) every 1 min for 10 min.

***Ex vivo* DPP-IV Activity Assay.** A volume of 40 μL of serum samples was loaded in each well of the black 96-well plates where RADA16-Lup1 and RADA16-Soy1 (100 μM) nanogels were present. Samples were then incubated for 24 h at 37 °C. The day after, 100.0 μL of DPPIV substrate at the concentration of 50.0 μM in PBS (Ca^{2+}/Mg^{2+} free) were added in each well and the fluorescence signals (ex./em. 350/450 nm) were measured using the Synergy H1 every 1 min for 10 min.

Determination of Lup1 and Soy1 Peptides release from the Nanogels. The peptide leaking from the nanogels as a function of time was measured dissolving the nanogles in PBS and measuring the concentrations of released peptides after 60, 180, 360 min of incubation by using a method previously described.[26] Briefly, a sterile solution of peptone from casein at 10 mg mL^{-1} in water was prepared and used as standard for the calibration curves. Reaction mixtures containing 9.5 μL of the solutions of released Lup1 and Soy1 or peptone solution, 90.5 μL water, 95 μL NaOH 6% (w/w) in water, and 9.5 μL of active reagent (containing 0.6 M sodium citrate, 0.9 M sodium carbonate, and 0.07 M copper sulfate, 2.4 M NaOH, pH 10.6) were prepared, incubated for 15 min at RT, and the absorbance was measured at 330 nm using the Synergy H1.

Statistically Analysis. Statistical analyses were carried out by t-student and One-way ANOVA using Graphpad Prism 6 (Graphpad, La Jolla, CA, USA). Values were expressed as means ± s.d. of three independent experiments, each experiment was performed in triplicate; P-values < 0.05 were

considered to be significant.

RESULTS

Assembly Mechanisms of Lup1 and Soy1 Nanogels. Soy1 and Lup1 nanogels were prepared by dissolving the purified RADA16 in distilled water at the concentration of 10 mg mL^{-1} and adding each peptide in the concentration range from 0.1 to 1000 μM). The nanogels formation was stimulated using a solvent-triggered approach (i.e. 1X PBS Ca^{2+}/Mg^{2+} free, isotonic saline solution with ionic strength 0.09%, DMEM). The achievement of a nanogel state was confirmed by the vial-inversion test, where the self-assembled structure can hold its own weight (Figure 1B). Both RADA16-Lup1 and RADA16-Soy1 solutions are fully miscible and appear as a viscous-liquid: upon addition of 1X PBS, the solutions gradually turn to translucent gels in less than 2 h at RT.

Biomechanical Behavior of Lup1 and Soy1 Nanogels. A thorough investigation of the RADA16-Lup1 and RADA16-Soy1 gelation process was performed using oscillatory shear rheological experiments. The rheological measurements of the storage (*G'*) and loss (*G"*) moduli are commonly used to characterize viscoelastic and mechanical properties of soft materials. *G'* reflects the stiffness of the biomaterial, while *G"* represents the energy dissipated during the oscillatory test and correlates with the liquid-like response of the hydrogel. The ratio between *G'* and *G"* provides insights of the viscoelastic profile of the material, i.e. whether it behaves as a viscous liquid (*G'*<*G"*) or as an elastic solid (*G'*>*G"*).

All pre-assembled solutions were monitored *via* time-sweep tests for 10 h after exposure to a pH shift (See Materials and Methods for further details). By monitoring the temporal evolution of *G'* and *G"*, the gelation kinetics and the increasing nanogel stiffness of both RADA16-Lup1 and RADA16-Soy1 were observed (Figure 2A). The gelation kinetics of both nanogels display typical hydrogel-like profiles;[27] furthermore, since they are β-sheet rich peptides (as it will be discussed in the next

paragraph), the growing presence of β-structures leads to the formation of an entangled fibrous network that provides increased *G'* values.[28] The progression of *G'* and its comparison with *G"* was also monitored *via* frequency sweep test performed at the linear viscoelastic region of each sample (Figure 2B). The trend of *G'* and *G"* for each nanogel showed the typical profile of soft hydrogels,[29] featuring a predominant solid-elastic behavior (*G'*) as compared to the viscous component (*G"*): indeed *G'* values were generally one order of magnitude greater the *G"*.

Also, *G'/G"* remained relatively constant along the tested frequency range (0.1-100 Hz) with RADA16-Soy1 displaying an average *G'* value of 1826 Pa and RADA16-Lup1 of 591.5 Pa.

Failure strain/stress tests were performed within the linear viscoelasticity region to assess material failure when subjected to a linear stress/strain progression at +25 °C. As expected, both nanogels, yielding to a soft hydrogel, showed a strain-to-failure of 8.87% and 9.24%, respectively, for RADA16-Soy1 and RADA16-Lup1 (Figure 2C), while stress failure occurred at stresses of 49.2 Pa for RADA16-Soy1 and 25.6 Pa for RADA16-Lup1 (Figure 2D).

Injectability and Shear-Thinning Propensity of Lup1 and Soy1 Nanogels. Over the past decades, injectable hydrogels have become more and more popular for their ability to be delivered *via* minimally invasive approaches. The injectability of shear-thinning hydrogels plays a key role in enabling their minimally invasive delivery: indeed, shear-thinning hydrogels are being investigated in various biomedical applications including drug delivery[30-32] and tissue regeneration.[25, 29, 33]

Here, to evaluate the propensity of nanogels to recover their initial viscosity after injection, the thixotropy of RADA16-Lup1 and RADA16-Soy1 was investigated using either quantitative (shear-thinning test) or qualitative techniques (*in vitro* injection test).[34] In the shear-thinning test the injection conditions were simulated through a series of constant shear rate tests: 1) (0.01 s^{-1}) low shear rate (stationary plunger); 2) (5.30 s^{-1}) shear rate inside the syringe barrel; 3) (1000 s^{-1}), high shear rate inside the needle; 4) (5.30 s^{-1}) shear rate out of the needle; 5) (0.01 s^{-1}) low shear rate after the injection. Both nanogels exhibited a fast recovery after injection simulation (Figure 3A). This

displays their ability to transition from a predominantly elastic material to a predominantly viscous one, and demonstrates their rapid properties of shear-thinning.

The qualitative assessment of nanogels injectability was performed by loading them into syringes and injecting into PBS, since this buffer mimics physiological pH and osmolarity (see Supplementary Video). A dye was used to visualize the nanogel during these assessments. Usually shear-thinning materials retain their shape after injection and, if dyed, should not lead to any dispersion of materials or dye into the PBS solution. Even here, both RADA16-Lup1 and RADA16-Soy1 demonstrate rapid self-thinning propensity after injection with no dispersion of payload (Figure 3B).

Tracking Secondary Structures using FT-IR. The attenuated total reflection (ATR) Fourier transform infrared (FT-IR) spectroscopy was utilized to probe the secondary structures of assembled RADA16-Lup1 and RADA16-Soy1 nanogels. The FT-IR spectra of both nanogels mostly overlap over the range of 1200-2000 cm^{-1} suggesting that they assume the same secondary structure (Figure 4A). Both FT-IR spectra display peaks at ~1630 cm^{-1} and ~1695 cm^{-1} (Amide I region), typically associated to β-sheet signatures. Moreover, in the Amide II region (1480-1575 cm^{-1}), a β-sheet aggregation for all tested nanogels was confirmed by the presence of the peak centered around at 1530 cm^{-1}, which is directly related to CN stretching and NH bending of peptide-backbone conformation.

Furthermore, in order to get a better insight on the RADA16-Lup1 and RADA16-Soy1 capacity of forming cross-β fibrils structures, the Thioflavin T (ThT) spectroscopy assay was carried out (Figure 4B). This assay enables to evaluate the cross-β structures and fibril formation of materials, since β-rich structures feature ThT-binding sites. Basically, ThT has a weak fluorescence in aqueous environment, with excitation and emission bands centered at approximately 350 nm and 440 nm, respectively. Upon binding to β-rich fibrils, bathochromic shifts of both excitation and emission to 440 nm and ~490 nm, respectively, are observed. The emission intensity at ~490 nm is assumed to

be directly proportional to the quantity of cross-β fibrils present in the sample. When the probe ThT was applied to both RADA16-Lup1 and RADA16-Soy1, a characteristic fluorescence emission at ~490 nm confirmed that the nanogels had adopted a similar cross-β-sheet conformation.

Overall, both FT-IR and ThT results clearly indicate that both nanogels self-aggregated into stable cross-β-sheets structures.

Lup1 and Soy1 Nanogels enhance the DPP-IV inhibitory Activity. In order to evaluate the ability of Lup1 and Soy1 nanogels to modulate the DPP-IV activity, *in situ* and *ex vivo* experiments were performed on human intestinal cells and human serum, respectively (Figure 5A-C). For the *in situ* experiment, a total of $5x10^4$/well Caco-2 cells were seeded directly on top of the nanogels in which Lup1 and Soy1 peptides were encapsulated in the concentration range of 0.1-1000 µM. After 24 h of incubation, 50.0 µM of Gly-Pro-AMC were added in each well and the effect of Lup1 and Soy1 peptides was evaluated measuring the fluorescence signal at 450 nm within 10 min. Both peptides encapsulated in the nanogels dropped the DPP-IV activity with a dose-response trend with IC_{50} values by 28.1±0.47 µM and 60.4 ±0.46 µM, respectively, for Lup1 and Soy1 (Figure 5A).

Subsequently, the effects of RADA16-Lup1 and RADA16-Soy1 on circulating DPP-IV activity were assessed by *ex vivo* experiments using human serum. In this case, the nanogels were prepared encapsulating 100 µM of each peptide and the serum samples were incubated with each nanogel for 24 h at 37°C. The following day, the fluorescent DPP-IV substrate (Gly-Pro-AMC) was added and the fluorescence signals were measured for 4 min. Figure 4B shows clearly that the circulating DPP-IV activity increases as a function of time with a linear trend after the addition of the substrate and that it is significantly reduced in the presence of the encapsulated peptides. Comparing the percent activity reduction at 2 min (Figure 5B), RADA16-Lup1 drops the circulating DPP-IV activity by 29±2.4% and RADA16-Soy1 by 25±3.1% *vs* control samples (RADA alone).

Lup1 and Soy1 Nanogels Release and Activity. In order to measure the release of Lup1 and Soy1

303 from the nanogels as a function of time, the nanogels containing 100 μM peptides were mixed with
304 PBS and after 60, 180, and 360 min of incubation the amount of each released peptide was
305 quantified.[35] This experiment showed that both peptides are released from the hydrogel but with
306 different trends. In details, the concentrations of released Lup1 were 0.06±0.01, 0.11±0.03, and
307 0.31±0.01 μg μL^{-1} after 60, 180, and 360 min, whereas those of released Soy1 were 0.17±0.04,
308 0.27±0.003, and 0.33±0.07 μg μL^{-1}, respectively (Figure 6A). In parallel, the inhibitory activities of
309 RADA16-Lup1 and RADA16-Soy1 nanogels on DPP-IV were assessed *ex vivo* for a tentative
310 evaluation of the correlation between activity and delivery. Figure 6B and 6C highlight that RADA-
311 Lup1 drops the circulating DPP-IV activity by 33.9±1.3%, 41.6±3.0%, and 49.5±1.2% after 60, 180,
312 and 360 min, whereas RADA-Soy1 by 34.6±4.5, 49.2±3.8, and 49.7±3.0%.
313

DISCUSSION

Lup1 and Soy1 are two peptides, deriving from plant proteins, that have the ability to diminish the activity of DPP-IV in different experimental models. Indeed, the scientific approach used by us for studying these peptides is unique in the panorama of food-derived peptides with DPP-IV inhibitory activity. Initially, we have demonstrated that both Lup1 and Soy1 drop *in vitro* the activity of the enzyme with a dose-response trend and IC_{50} values equal to 228 and 106 µM, respectively. These values are in line with literature that provides many examples of food-derived peptides able to inhibit DPP-IV.[8, 36-38] However, most published studies have the relevant limitation of being based almost exclusively on *in vitro* enzymatic assays that do not take into account several factors that might influence a peptide bioactivity, such as the resistance to digestive enzymes, the metabolism, and the absorption. In particular, the brush border (BB) of the microvilli is the first physiological barrier that food-derived bioactive peptides encounter. For a correct characterization of their inhibitory properties, it would be certainly necessary to use an experimental model that takes into account the actual characteristics of the intestinal environmental.

We have therefore used a suitable model[13] based on alive Caco-2 cells and have demonstrated that both Lup1 and Soy1 drop the DPP-IV activity even in the presence of BB proteolytic activity, maintaining their dose-response behavior and displaying IC_{50} values equal to 208 and 223 µM. Whereas the calculated IC_{50} of Lup1 was substantially in agreement with that obtained in the *in vitro* assay, Soy1 resulted to be about 2-folds less active *in situ* than *in vitro*. The different behavior of these peptides may be explained by their different stability in the presence of the complex intestinal environment.[15] Thus, the reduced *in situ* DPP-IV inhibitory activity of Soy1 is likely due to its metabolic degradation by the hydrolytic activity of BB membrane peptidases.

In light with these observations, it is clear that the low stability and bioavailability are major concern for the development of practical applications of these bioactive peptides. In order to overcome these problems, it was decided to develop a well-designed and controlled delivery system based on self-

assembling peptides. The ionic self-complementary RADA16 peptide is known to possess a strong propensity to spontaneously self-assemble into ordered nanofibrous structures upon exposure to external stimuli (e.g., pH, temperature, monovalent or divalent electrolyte ions).[39] Typically, the driving forces that governs RADA16 self-assemblying in water arises from three major energy contributions: hydrophobic interactions, hydrogen bonding among the peptide segments, and electrostatic repulsions between the charged amino acids.[21] These forces tend to promote the aggregation of RADA16 molecules to form, at the macroscale level, highly hydrated hydrogels containing up to 99.5% (w/v) water.

RADA16 has been shown to have excellent characteristics owing to the unique β-sheet secondary structure, which is the main factor for the formation of stable nanofibrous hydrogels, and it is also determinant for its performance including mechanical properties (i.e. stiffness, strain and stress resistance), shear-thinning properties, and stimuli-responsiveness. It was easy to trap both Soy1 and Lup1 peptides inside the nanofibrous domains of the RADA16 structure without affecting the macromolecular organization and facilitating their slow and sustained release from the nanogel. Indeed, the *in situ* activities of Lup1 and Soy1 in Caco-2 cells were enhanced by 7.3 and 3.7 folds when they were entrapped inside the entangled nanofibrous domains of the hydrogels in respect to their plain solutions (Figure 5A).

The encapsulation in the RADA16 hydrogel has a positive effect also circulating DPP-IV. In fact, whereas free Lup1 and Soy1 peptides impair the activity of this enzyme in human serum by 18.1% and 27.7% at 100 μM, respectively,[13] at the same concentration RADA-Lup1 nanogel impaired the DPP-IV activity by 29% and RADA-Soy1 by 25% (Figure 5C). In this case, apparently the encapsulation improved only the Lup1 activity, suggesting that Soy1 is more susceptible to the degradation by the proteases circulating in human serum, which is a very complex environment.

Overall, our findings suggest that the encapsulation of both peptides within the RADA16 hydrogel provides not only higher resistance towards the proteases but also a higher bioavailability. For this reason, it was supposed that when Lup1 and Soy1 are embedded within nanogels, they are slowly

released allowing their interaction with the DPP-IV catalytic site. In order to confirm this hypothesis, a kinetic study of their release after 60, 180, and 360 min of incubation was performed quantifying the released peptides with an experimental method already used by us in different situations.[40] Figure 6A clearly underlines that Lup1 is regularly delivered from the RADA16 hydrogel during all the 360 min, whereas Soy1 is rapidly released in the first 180 min, but remains relatively constant afterwards. These differences appear to be in agreement with the RADA-Lup1 and RADA-Soy1 activity on circulating DPP-IV on human serum samples (Figure 6B-C). In fact, the activity of RADA16-Lup 1 increases regularly as a function of time, whereas the activity of RADA16-Soy1 increases until 180 min and then remains practically constant. The different physico-chemical properties of these peptides have certainly a major role here: in particular, the faster release of Soy1 may be linked to its minor hydrophobicity (Soy1 hydrophobicity +8.40 Kcal mol^{-1}, Lup1 hydrophobicity +14.71 Kcal mol^{-1}). This may explain why peptide Soy1 may more easily escape from the entangled nanofibrous domains of the hydrogels. In addition, the faster degradation of Soy1 in respect to Lup1 by active serum proteases may negatively affect the bioactivity at longer time.

In conclusion, for the first time here a nanotechnological approach based on SAPs has been combined with bioactive food-derived peptides in order to produce nanogels active as DPP-IV inhibitors. This innovative approach may represent the dawn of a new generation of nano-materials capable of delivering nutraceuticals as well as pharmaceuticals in a controlled and harmlessly manner.

Abbreviations and Nomenclature

AMC, amido-4-methylcoumarin hydrobromide; **BB**, brush border; **DMEM**, Dulbecco's modified Eagle's medium; **TFA**, trifluoroaceticacid; **TIS**, triisopropylsilane; **DPP-IV,** Dipeptidyl peptidase IV; **FBS**, foetal bovine serum; **GLP-1**, glucagon-like peptide-1; **GIP**, gastrointestinal insulinotropic peptide; PBS, phosphate buffered saline; **RFU**, relative fluorescence unit; **RT**, room temperature; **SAPs,** self-assembling peptides; **T2DM**, type 2 diabetes.

ORCID

R. Pugliese https://orcid.org/0000-0001-7669-4457 ;

F. Gelain https://orcid.org/0000-0002-2624-5853 ;

A. Arnoldi https://orcid.org/0000-0002-0987-3014 ;

C. Lammi https://orcid.org/0000-0002-7428-4486 ;

Author Contributions

C.L. and R.P. conceived the project and designed the experiments. C.L. took care all *in situ*, and *ex vivo*, and release tests, while R.P. and F.G synthesized the RADA16 peptide and carried out all structural and biomechanical experiments. C.L., A.A, and R.P wrote the manuscript. All authors critically reviewed the paper, and have approved the final article.

Acknowledgment

We are indebted to Carlo Sirtori Foundation (Milan, Italy) for having provided part of equipment used in this experimentation.

Supporting Information

The Supporting Information, which is available free of charge on the ACS Publications website at DOI: XXX, provides Table S1, Video, and a more detailed description of material and methods section

Notes

The authors declare no competing financial interest.

References

1. Abbott, C. A.; Baker, E.; Sutherland, G. R.; McCaughan, G. W., Genomic organization, exact localization, and tissue expression of the human CD26 (dipeptidyl peptidase IV) gene. *Immunogenetics* **1994,** *40* (5), 331-338.

2. Röhrborn, D.; Wronkowitz, N.; Eckel, J., DPP4 in Diabetes. *Front Immunol* **2015,** *6*, 386.

3. Nargis, T.; Chakrabarti, P., Significance of circulatory DPP4 activity in metabolic diseases. *IUBMB Life* **2018,** *70* (2), 112-119.

4. Lacroix, I. M. E.; Li-Chan, E. C. Y., Dipeptidyl peptidase-IV inhibitory activity of dairy protein hydrolysates. *Int Dairy J* **2012,** *25* (2), 97-102.

5. Nauck, M. A.; Baller, B.; Meier, J. J., Gastric inhibitory polypeptide and glucagon-like peptide-1 in the pathogenesis of type 2 diabetes. *Diabetes* **2004,** *53 Suppl 3*, S190-196.

6. Doupis, J.; Veves, A., DPP4 inhibitors: a new approach in diabetes treatment. *Adv Ther* **2008,** *25* (7), 627-43.

7. Dicker, D., DPP-4 inhibitors: impact on glycemic control and cardiovascular risk factors. *Diab Care* **2011,** *34 Suppl 2*, S276-278.

8. Lacroix, I. M.; Li-Chan, E. C., Isolation and characterization of peptides with dipeptidyl peptidase-IV inhibitory activity from pepsin-treated bovine whey proteins. *Peptides* **2014,** *54*, 39-48.

9. Jao, C. L.; Hung, C. C.; Tung, Y. S.; Lin, P. Y.; Chen, M. C.; Hsu, K. C., The development of bioactive peptides from dietary proteins as a dipeptidyl peptidase IV inhibitor for the management of type 2 diabetes. *Biomedicine (Taipei)* **2015,** *5* (3), 14.

10. Power, O.; Nongonierma, A. B.; Jakeman, P.; FitzGerald, R. J., Food protein hydrolysates as a source of dipeptidyl peptidase IV inhibitory peptides for the management of type 2 diabetes. *Proc Nutr Soc* **2014,** *73* (1), 34-46.

11. Lammi, C.; Zanoni, C.; Arnoldi, A.; Vistoli, G., Peptides derived from soy and lupin protein as Dipeptidyl-Peptidase IV inhibitors: *In vitro* biochemical screening and *in silico* molecular modeling study. *J Agric Food Chem* **2016,** *64* (51), 9601-9606.

12. Zanoni, C.; Aiello, G.; Arnoldi, A.; Lammi, C., Investigations on the hypocholesterolaemic activity of LILPKHSDAD and LTFPGSAED, two peptides from lupin beta-conglutin: Focus on LDLR and PCSK9 pathways. *J Funct Foods* **2017,** *32*, 1-8.

13. Lammi, C.; Bollati, C.; Ferruzza, S.; Ranaldi, G.; Sambuy, Y.; Arnoldi, A., Soybean- and lupin-derived peptides inhibit DPP-IV activity on in situ human intestinal Caco-2 cells and ex vivo human serum. *Nutrients* **2018,** *10* (8).

14. Lammi, C.; Aiello, G.; Vistoli, G.; Zanoni, C.; Arnoldi, A.; Sambuy, Y.; Ferruzza, S.; Ranaldi, G., A multidisciplinary investigation on the bioavailability and activity of peptides from lupin protein. *J Funct Foods* **2016,** *24*, 297-306.

15. Aiello, G.; Ferruzza, S.; Ranaldi, G.; Sambuy, Y.; Arnoldi, A.; Vistoli, G.; Lammi, C., Behavior of three hypocholesterolemic peptides from soy protein in an intestinal model based on differentiated Caco-2 cell. *J Funct Foods* **2018,** *45*, 363-370.

16. Lopalco, A.; Denora, N., Nanoformulations for drug delivery: safety, toxicity, and efficacy. *Methods Mol Biol* **2018,** *1800*, 347-365.

17. Park, K., Controlled drug delivery systems: past forward and future back. *J Control Release* **2014,** *190*, 3-8.

18. Gelain, F.; Unsworth, L. D.; Zhang, S., Slow and sustained release of active cytokines from self-assembling peptide scaffolds. *J Control Release* **2010,** *145* (3), 231-239.

19. Koutsopoulos, S.; Unsworth, L. D.; Nagai, Y.; Zhang, S., Controlled release of functional proteins through designer self-assembling peptide nanofiber hydrogel scaffold. *Proc Natl Acad Sci U S A* **2009,** *106* (12), 4623-8.

20. Bolat, G.; Abaci, S.; Vural, T.; Bozdogan, B.; Denkbas, E. B., Sensitive electrochemical detection of fenitrothion pesticide based on self-assembled peptide-nanotubes modified disposable pencil graphite electrode. *J. Electroanal. Chem* **2018,** *809*, 88-95.

21. Pugliese, R.; Gelain, F., Peptidic biomaterials: from self-assembling to regenerative medicine. *Trends Biotechnol* **2017,** *35* (2), 145-158.

22. Tao, K.; Makam, P.; Aizen, R.; Gazit, E., Self-assembling peptide semiconductors. *Science* **2017,** *358* (6365).

23. Zhang, S.; Holmes, T.; Lockshin, C.; Rich, A., Spontaneous assembly of a self-complementary oligopeptide to form a stable macroscopic membrane. *Proc Natl Acad Sci U S A* **1993,** *90* (8), 3334-3338.

24. Lammi, C.; Bollati, C.; Gelain, F.; Arnoldi, A.; Pugliese, R., Enhancement of the stability and anti-DPPIV activity of hempseed hydrolysates through self-assembling peptide-based hydrogels. *Front Chem* **2019,** *doi: 10.3389/fchem.2018.00670*.

25. Pugliese, R.; Fontana, F.; Marchini, A.; Gelain, F., Branched peptides integrate into self-assembled nanostructures and enhance biomechanics of peptidic hydrogels. *Acta Biomater* **2018,** *66*, 258-271.

26. Levashov, P. A.; Sutherland, D. S.; Besenbacher, F.; Shipovskov, S., A robust method of determination of high concentrations of peptides and proteins. *Anal Biochem* **2009,** *395* (1), 111-112.

27. Raspa, A.; Saracino, G. A. A.; Pugliese, R.; Silva, D.; Cigognini, D.; Vescovi, A.; Gelain, F., Complementary Co-assembling Peptides: From In Silico Studies to In Vivo Application. *Adv Funct Mater* **2014,** *24* (40), 6317-6328.

28. Yan, C.; Pochan, D. J., Rheological properties of peptide-based hydrogels for biomedical and other applications. *Chem Soc Rev* **2010,** *39* (9), 3528-3540.

29. Cigognini, D.; Silva, D.; Paloppi, S.; Gelain, F., Evaluation of mechanical properties and therapeutic effect of injectable self-assembling hydrogels for spinal cord injury. *J Biomed Nanotechnol* **2014,** *10* (2), 309-323.

30. Purcell, B. P.; Lobb, D.; Charati, M. B.; Dorsey, S. M.; Wade, R. J.; Zellars, K. N.; Doviak, H.; Pettaway, S.; Logdon, C. B.; Shuman, J. A.; Freels, P. D.; Gorman, J. H.; Gorman, R. C.; Spinale, F. G.; Burdick, J. A., Injectable and bioresponsive hydrogels for on-demand matrix metalloproteinase inhibition. *Nat Mater* **2014,** *13* (6), 653-661.

31. Dimatteo, R.; Darling, N. J.; Segura, T., In situ forming injectable hydrogels for drug delivery and wound repair. *Adv Drug Deliv Rev* **2018,** *127*, 167-184.

32. Wang, L. L.; Sloand, J. N.; Gaffey, A. C.; Venkataraman, C. M.; Wang, Z.; Trubelja, A.; Hammer, D. A.; Atluri, P.; Burdick, J. A., Injectable, Guest-Host Assembled Polyethylenimine Hydrogel for siRNA Delivery. *Biomacromolecules* **2017,** *18* (1), 77-86.

33. Pugliese, R.; Marchini, A.; Saracino, G. A. A.; Zuckermann, R. N.; Gelain, F., Cross-linked self-assembling peptide scaffolds. *Nano Research* **2018,** *11* (1), 586-602.

34. Chen, M. H.; Wang, L. L.; Chung, J. J.; Kim, Y. H.; Atluri, P.; Burdick, J. A., Methods To Assess Shear-Thinning Hydrogels for Application As Injectable Biomaterials. *ACS Biomater Sci Eng* **2017,** *3* (12), 3146-3160.

35. Goa, J., A micro biuret method for protein determination. Determination of total protein in cerebrospinal fluid. *Scand J Clin Lab Invest* **1953,** *5*, 218-222.

36. Nongonierma, A. B.; Mooney, C.; Shields, D. C.; FitzGerald, R. J., In silico approaches to predict the potential of milk protein-derived peptides as dipeptidyl peptidase IV (DPP-IV) inhibitors. *Peptides* **2014,** *57*, 43-51.

37. Nongonierma, A. B.; Paolella, S.; Mudgil, P.; Maqsood, S.; FitzGerald, R. J., Identification of novel dipeptidyl peptidase IV (DPP-IV) inhibitory peptides in camel milk protein hydrolysates. *Food Chem* **2018,** *244*, 340-348.

38. Lacroix, I. M. E.; Li-Chan, E. C. Y., Food-derived dipeptidyl-peptidase IV inhibitors as a potential approach for glycemic regulation - Current knowledge and future research considerations. *Trends Food Sci & Technol* **2016,** *54*, 1-16.

39. Yokoi, H.; Kinoshita, T.; Zhang, S., Dynamic reassembly of peptide RADA16 nanofiber scaffold. *Proc Natl Acad Sci U S A* **2005,** *102* (24), 8414-8419.

40. Lammi, C.; Zanoni, C.; Scigliuolo, G. M.; D'Amato, A.; Arnoldi, A., Lupin peptides lower low-density lipoprotein (LDL) cholesterol through an up-regulation of the LDL receptor/sterol regulatory element binding protein 2 (SREBP2) pathway at HepG2 cell line. *J Agric Food Chem* **2014,** *62* (29), 7151-7159.

Funding sources

The work described and performed by R. P. and F. G. was funded by the "Ricerca Corrente" funding granted by the Italian Ministry of Health and by the "5 × 1000" voluntary contributions. The work described and carried out by C.L. and A. A. was supported in part by the ERA-NET project DISCOVERY: "Disaggregation of conventional vegetable press cakes by novel techniques to receive new products and to increase the yield". Project code SUSFOOD2-ID:101

FIGURE CAPTIONS.

Figure 1. Self-assembly of RADA16, Soy1 and Lup1 nanogels. (A) Chemical structures of RADA16, Soy1 and Lup1. (B) Gel formation of RADA16-Soy1 and RADA16-Lup1 *via* solvent-triggered approach (the Figure shows only Soy1). (C) Cartoon modeling of RADA16-Soy1 and RADA16-Lup1 hydrogels. The RADA16 network of nanofibers is shown in blue, while peptides Soy1 and Lup1 are in yellow and light gray, respectively.

Figure 2. Biomechanical characterization of RADA16-Lup1 and RADA16-Soy1 nanogels. (A) Nanogels monitored *via* a 10 h time-sweep test and (B) *via* a frequency sweep test (0.1-1000 Hz): the typical hydrogel profile was confirmed for both peptides, displaying a predominant solid-like behavior (*G'*) (solid dots) compared with the viscous component (*G"*) (empty dots). Strain (C) and stress (D) failure tests: both nanogels, behaving as soft hydrogels, showed strain-to-failures similar to other SAP-based hydrogels.

Figure 3. Injectability assessment of RADA16-Soy1 and RADA16-Lup1 nanogels. (A) The thixotropic test. It suggests a shear-thinning behavior of both RADA16-Soy1 (green) and RADA16-Lup1 (red), thanks to the rapid recovery of the initial viscosity after simulated injection. (B) Manual injections of RADA16-Soy1 nanogel into PBS from 30G X ½ (diameter: 0.3 mm) insulin syringe. it demonstrates shear-thinning propensity and no dispersion of material after injection. (Scale bar = 50 mm).

Figure 4. Supramolecular organization of assembled RADA16-Lup1 and RADA16-Soy1 nanogels. (A) ATR-FT-IR spectra of RADA16-Soy1 (green) and RADA16-Lup1 (red) nanogels: they display typical β-sheet signature in Amide I (1600-1700 cm^{-1}) and Amide II (1480-1575 cm^{-1}) regions. (B) ThT emission spectra of RADA16-Soy1 (green) and RADA16-Lup1 (red) nanogels: they show an affinity for ThT ascribable to the presence of cross-β fibril structures.

Figure 5. **DPP-IV inhibitory activity of RADA16-Lup1 and RADA16-Soy1 hydrogels**. A) RADA16-Lup1 and RADA16-Soy1 hydrogels reduce *in situ* the DPPIV activity in non-differentiated human Caco-2 cells with a dose-response trend and IC_{50} values equal to 28.1±0.47 μM and 60.4±0.46 μM, respectively. Data represent the mean±s.d. of three independent experiments performed in triplicate. the mean of the calculated IC_{50} have been compared by t-student and results suggest that RADA16-Lup1 is more active than RADA16-Soy1 (* $p < 0.05$). B) Circulating DPP-IV activity increases as a function of the time with a linear trend after the addition of fluorescent substrate (Gly-Pro-AMC, 50 μM) (black line), but it is significantly reduced in the presence of 100 μM RADA16-Lup1 (red line) or RADA16-Soy1 (green line). Data represent the mean±s.d. of three independent experiments performed in triplicate. C) At time = 2 min, RADA16-Lup1 and RADA16-Soy1 hydrogels decrease the circulating DPPIV activity by 29±2.4% and 25±3.1% respectively, versus plain RADA16. Data represent the mean±s.d. of three independent experiments performed in triplicate and they were analyzed by the one-way analysis of variance (ANOVA), **** $p < 0.00001$. The mean values of RADA16-Lup1 and RADA16-Soy1 have been compared by t-student, suggesting that RADA16-Lup1 is more active than RADA16-Soy1 (* $p < 0.05$)

Figure 6. Release and activity of RADA16-Lup1 and RADA16-Soy1 as a function of time. A) RADA16-Lup1 and RADA16-Soy1 were released from the hydrogels with a different kinetics after 60, 180, and 360 min. B) RADA16-Lup1 and C) RADA-Soy1 dropped the DPP-IV activity in human serum samples as a function of the time. Data in all panels have been analyzed by the one-way analysis of variance (ANOVA), *$p < 0.05$; **** $p < 0.00001$

Figure 1

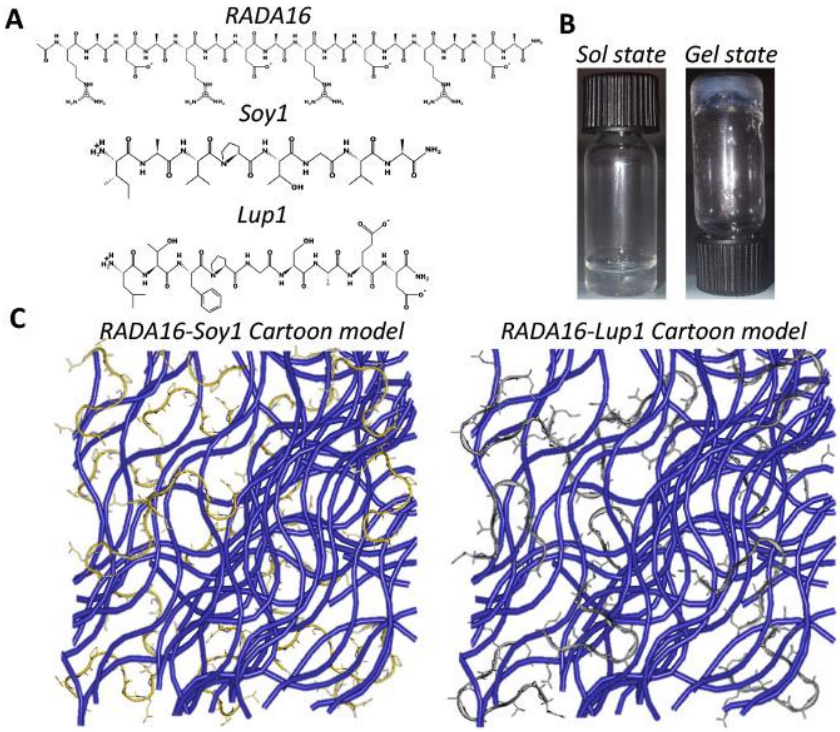
A
RADA16
Soy1
Lup1
B
Sol state
Gel state
C
RADA16-Soy1 Cartoon model
RADA16-Lup1 Cartoon model

Figure 2

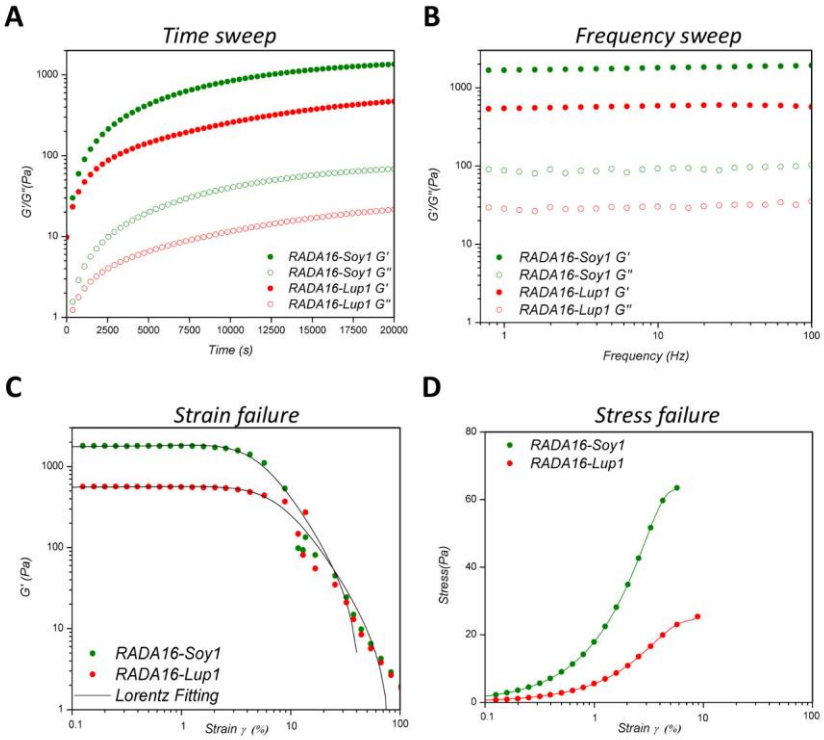
A
Time sweep
G'/G''(Pa)
Time (s)
RADA16-Soy1 G'
RADA16-Soy1 G''
RADA16-Lup1 G'
RADA16-Lup1 G''
B
Frequency sweep
G'/G''(Pa)
Frequency (Hz)
RADA16-Soy1 G'
RADA16-Soy1 G''
RADA16-Lup1 G'
RADA16-Lup1 G''
C
Strain failure
G' (Pa)
Strain γ (%)
RADA16-Soy1
RADA16-Lup1
Lorentz Fitting
D
Stress failure
Stress(Pa)
Strain γ (%)
RADA16-Soy1
RADA16-Lup1

588 **Figure 3**
589

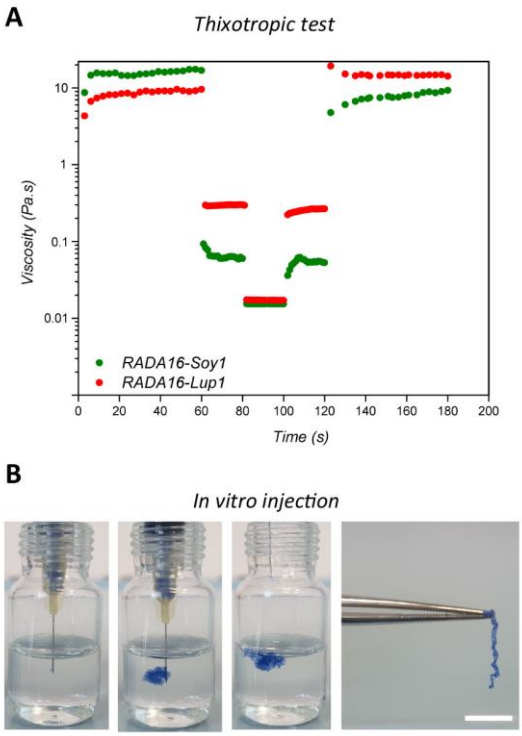

590
591

Figure 4

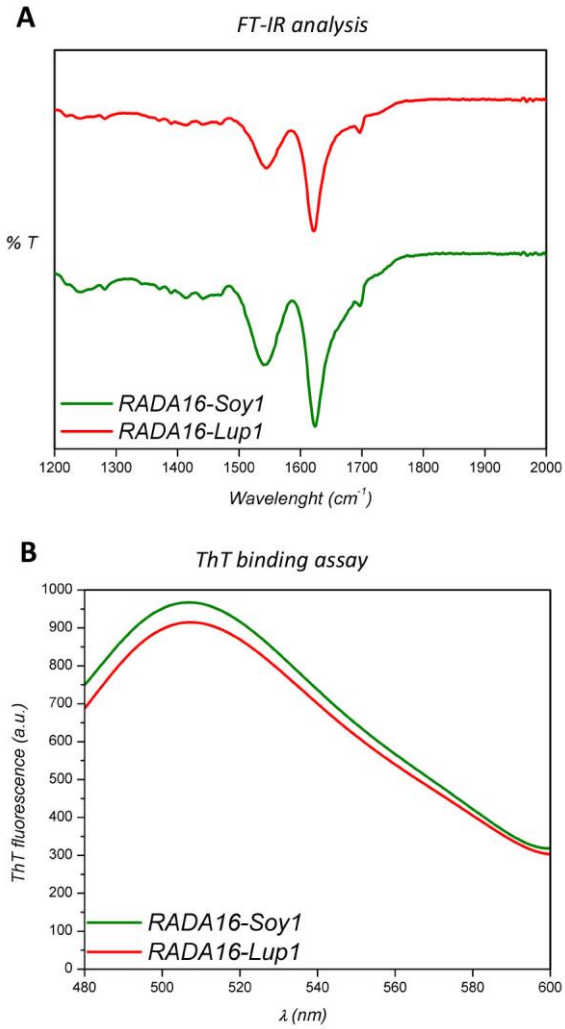
A
FT-IR analysis
% T
RADA16-Soy1
RADA16-Lup1
1200
1300
1400
1500
1600
1700
1800
1900
2000
Wavelenght (cm-1)
B
ThT binding assay
ThT fluorescence (a.u.)
1000
900
800
700
600
500
400
300
200
100
0
RADA16-Soy1
RADA16-Lup1
480
500
520
540
560
580
600
λ (nm)

Figure 5

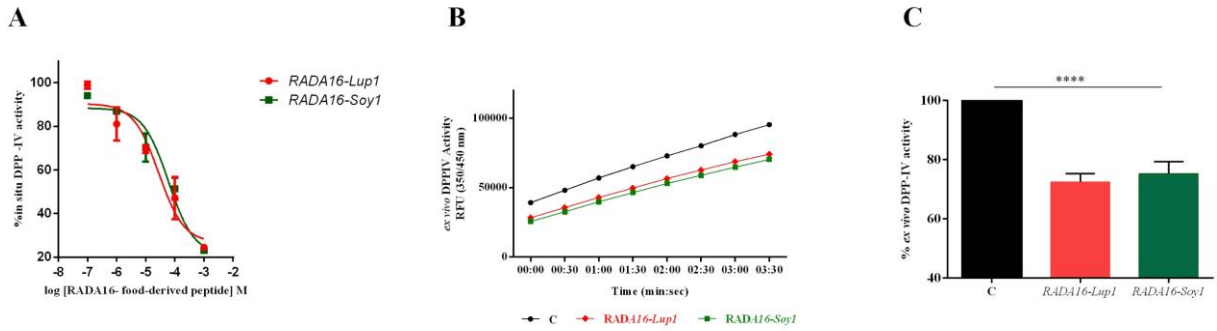
A
B
C
RADA16-Lup1
RADA16-Soy1
% in situ DPP -IV activity
log [RADA16- food-derived peptide] M
ex vivo DPPIV Activity
RFU (350/450 nm)
Time (min:sec)
C
RADA16-Lup1
RADA16-Soy1
% ex vivo DPP-IV activity
****

Figure 6

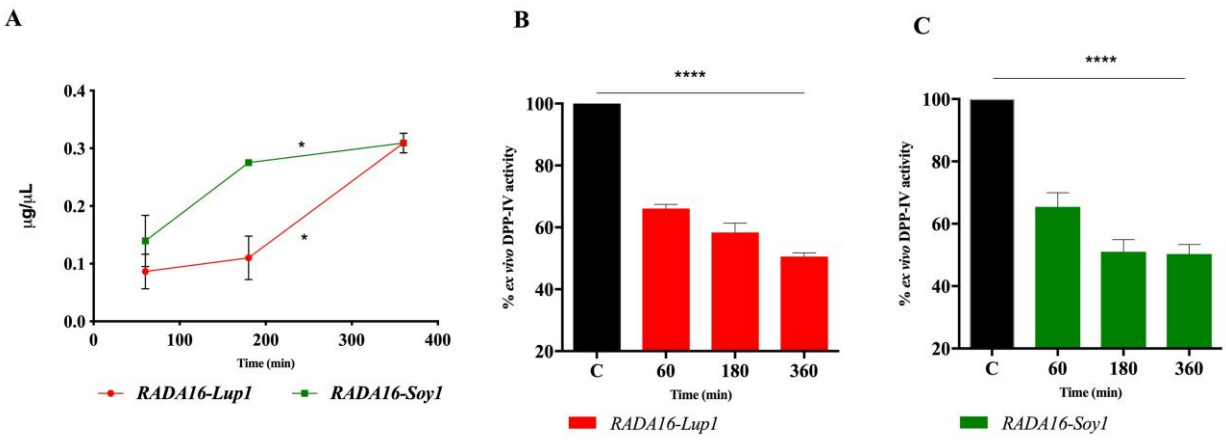
A
B
C
µg/µL
Time (min)
RADA16-Lup1
RADA16-Soy1
% ex vivo DPP-IV activity
****
C
60
180
360

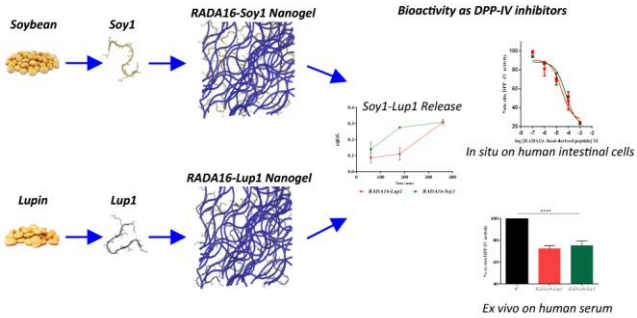
Soybean
Soy1
RADA16-Soy1 Nanogel
Bioactivity as DPP-IV inhibitors
Soy1-Lup1 Release
In situ on human intestinal cells
Lupin
Lup1
RADA16-Lup1 Nanogel
Ex vivo on human serum

TOC